





## Temperature-modulated magnetic skyrmion phases and transformations analysis from first-order reversal curve study

Calvin Ching Ian Ang , Weiliang Gan , Grayson Dao Hwee Wong , and Wen Siang Lew \*

*School of Physical and Mathematical Sciences, Nanyang Technological University, 21 Nanyang Link, Singapore 637371, Singapore*



(Received 1 February 2021; revised 9 March 2021; accepted 16 March 2021; published 6 April 2021)

We performed a temperature-modulated first-order reversal curve (FORC) study on a Pt/Co/Fe/Ir magnetic stack that exhibited a magnetic phase transition from isolated skyrmions to skyrmion lattice with increasing temperature. Using *in situ* magneto-optical Kerr imaging, a generalized description of domain transformations associated with the FORC distribution peaks at both their reversal and sweeping field are derived to allow for direct analysis from the FORC diagram. The sweeping field of the peak, which is commonly ignored in analysis, is identified as the process of domain propagation or nucleation towards terminal domain separation. This process is found to be essential in inducing magnetization irreversibility to reveal domain transformations. In addition, a model characterized by the FORC distribution peaks was developed to describe the transition from the isolated skyrmion to skyrmion lattice phase as well as to identify important field ranges for the transformations. This study establishes an intuitive form of analysis for the otherwise abstract data of FORC distribution for the characterization of magnetic skyrmions in the active field of skyrmionics.

DOI: [10.1103/PhysRevB.103.144409](https://doi.org/10.1103/PhysRevB.103.144409)

### I. INTRODUCTION

A magnetic skyrmion is a particlelike nanoscale magnetization state [1–5]. With promising potential as high-density information carriers, magnetic skyrmions are now actively investigated for applications such as memory [1,4,6–8], computational logic [9–12], and nonconventional computing systems [13–19]. Magnetic skyrmions stabilization requires the system to be favorable for nonparallel adjacent spins, which can be supported by the Dzyaloshinskii-Moriya interaction (DMI) [20–22] and dipolar interaction [23–25]. Ferromagnet (FM)-heavy metal (HM) multilayers commonly stabilize magnetic skyrmions at room temperature as strong interfacial-DMI is induced at the interface of an FM and HM with large spin-orbit coupling [26,27]. By having many repeats of these FM/HM layers in a stack, the dipolar interaction is enhanced to further stabilize the magnetic skyrmions [23,28].

As the stabilization of the magnetic skyrmion primarily depends on the energy cost of the twisting segment of its structure, the material parameter  $\kappa = \pi D/4\sqrt{AK}$  derived from domain wall energy is commonly used to characterize the stability of magnetic skyrmions in these materials, where  $D$  is DMI strength,  $A$  is the exchange stiffness, and  $K$  is the effective magnetic anisotropy strength [29,30]. As DMI strength increases and  $\kappa$  approaches unity, skyrmions become increasingly favorable and exist as isolated skyrmions. Above unity, the domain wall energy becomes negative resulting in the proliferation of skyrmions in a packed or lattice configuration [4,30,31]. While the composition and structure of the

multilayer can be tuned to obtain a material with the desired  $\kappa$  [26,32], prior studies also reported the increase in  $\kappa$  with temperature [33,34].

The first-order reversal curve (FORC) technique uses a combination of reversal field, sweeping field, and magnetization data to determine irreversible transitions. FORC is especially suitable for the characterization of magnetic skyrmions as it reveals magnetic states and transitions that are imperceivable in a major hysteresis loop or even by optical imaging techniques [35]. The application of the FORC technique was demonstrated to be useful in maximizing zero-field skyrmions based on the projected FORC distribution peaks onto the reversal fields [36,37]. A recent work extended its use to determine a pure Néel skyrmion structure from the disappearance of the FORC distribution trough [38]. Several earlier works also investigating similar bubble-stripe transitions attributed the FORC features to the fracturing of magnetic stripes and the skyrmion annihilation at the reversal field [35,39,40]. However, these analyses remain limited to the reversal field or a particular feature, leaving the sweeping field unexplored and its associated information about the system hidden.

In this Letter, we report the analysis of skyrmion transformations across both the reversal field and the sweeping field using Hall voltage measurement with *in situ* magneto-optical Kerr effect (MOKE) imaging. The domain transformation processes associated with each FORC distribution peak were identified and proved to be consistent across the skyrmion phases from isolated skyrmion to skyrmion lattice. The divergence in domain-domain separation from its terminal separation in the labyrinth state was revealed as the other key phenomena determining the FORC features. In addition, a model characterized by the FORC distribution peaks was developed to describe the transformations with increasing  $\kappa$

\*wensiang@ntu.edu.sg

from which the skyrmion phase and other useful field ranges can be deduced.

## II. METHODS

The material stack used in this experiment, Ta(5)/Ir(2)/[Pt(1)/Co(0.5)/Fe(0.5)/Ir(0.8)]<sub>2</sub>/Ta(5) (nominal layer thicknesses in nanometers) was chosen for the strong additive interfacial Dzyaloshinskii-Moriya interaction (i-DMI) by both the Pt/Co and Fe/Ir interfaces [26]. A thermally oxidized silicon wafer was used as the substrate. The material stack was deposited at room temperature using a magnetron sputtering system (AJA ATC-Orion 8) with a base pressure of  $8 \times 10^{-8}$  Torr or better. The materials Pt, Ta, Ir, and Fe were deposited via direct current at sputtering pressure of 2.0 mTorr and deposition rates of 0.68, 0.62, 0.37, 0.30 Å/s, respectively. Co was deposited via RF current at sputtering pressure of 3.0 mTorr and deposition rate of 0.26 Å/s. The top and bottom Ta(5) layers were deposited as a protective layer against oxidation and adhesion, respectively. The additional Ir underlayer was added to provide a similar interface for the repeating layers. The Hall cross device with  $20 \mu\text{m} \times 10 \mu\text{m}$  widths was subsequently fabricated using a combination of electron beam lithography (Raith e-line) and ion milling (AJA ion milling system with Hiden SIMS element detector) techniques.

Magnetic domain imaging was performed using the MagVision Kerr Imaging System which operates on the MOKE. In the polar configuration, the out-of-plane magnetization is probed and observed as different levels of brightness in the image. In the images, regions of lower brightness correspond to magnetization in the negative out-of-plane direction and vice versa. The images' color balance had been adjusted to offer the best contrast for qualitative analysis.

The out-of-plane magnetization used for FORC measurements was measured electrically by Hall voltage induced by the anomalous Hall effect across the Hall cross. Lock-in detection of Hall voltage was used to optimize the signal-to-noise ratio. A weak sensing current with the current density of  $2.3 \times 10^9 \text{ A/m}^2$  was used to probe the magnetization and was verified by MOKE images to cause a negligible effect on the magnetic domains.

Electrical measurements and MOKE imaging were performed *in situ*. However, a long exposure time was required to acquire a sufficiently clear MOKE image. Hence, the MOKE images for the hysteresis were taken with stepwise changes in the out-of-plane field instead of a continuous field sweep. For each of the images taken for the FORC sweep, the full sequence magnetic field sweep from the positive saturation field to the reversal field, and up to the desired final field was performed before a MOKE image is taken.

Temperature modulation was performed using a proportional-integral-derivative (PID) controlled thermoelectric cooler. The thermoelectric cooler was secured directly beneath the sample stage with a thermistor attached to the cooler. A microcontroller, Arduino Nano, was programmed to measure temperature using a precalibrated thermistor resistance, perform PID computations to control the output of the thermoelectric cooler, and maintain the desired temperature even with ambient fluctuations. A fluctuation

of less than  $0.1^\circ\text{C}$  was maintained for all measurements. By the measurement of the sample device resistance, the thermal conductivity from the thermoelectric cooler through the stage to the sample device was verified to be reliable with thermal equilibrium achieved in seconds.

## III. RESULTS AND DISCUSSION

### A. Temperature-modulated skyrmion phase transition

First, the supporting evidence for the transition of  $\kappa$  across unity occurring within the investigated small temperature range of  $18.0^\circ\text{C}$  to  $26.0^\circ\text{C}$  is presented. Figure 1(a) shows a decreasing enclosed area and gradient of the major hysteresis loop with temperature indicating the anisotropy shift towards the film plane. The linearly decreasing saturation Hall voltage with temperature relates to the expected decrease in saturation magnetization with temperature as shown in the inset of Fig. 1(a). The MOKE images of the demagnetized domains obtained using a decreasing alternating field sweep were analyzed by two-dimensional fast Fourier transforms to derive their corresponding domain periodicity shown in Fig. 1(b) [41–43]. While  $\kappa$  was not directly measured, the results in Figs. 1(a) and 1(b) remain aligned to that of a state with increasing  $\kappa$ . Figure 1(c) shows the MOKE images of magnetic domains after the out-of-plane field  $H_Z$  was swept from the positive saturation field to their labeled fields at temperatures of  $19.0^\circ\text{C}$  and  $26.0^\circ\text{C}$ , respectively. At  $19.0^\circ\text{C}$ , the labyrinth domains fracture into long stripe domains which receded into a sparse isolated skyrmion state with decreasing  $H_Z$ . In contrast, at  $26.0^\circ\text{C}$  and  $H_Z$  of 5.1 Oe, the domains formed a mix of short stripe segments and skyrmions domains instead of the labyrinth configuration. As  $H_Z$  was further decreased, these stripe segments fractured into the densely packed skyrmion lattice configuration. Hence, the temperature range of  $18.0^\circ\text{C}$  to  $26.0^\circ\text{C}$  used in this investigation encompasses the state of isolated skyrmion with  $\kappa < 1$  to skyrmion lattice  $\kappa > 1$ .

### B. First-order reversal curve distribution

FORCs were obtained following the sequence of magnetic field sweeps illustrated in Fig. 2(a). For a single FORC,  $H_Z$  is first swept from  $H_{\text{Sat}}$  that is sufficiently high to attain the saturated state, to a lower or negative field  $H_R$  following the blue dashed line shown in Fig. 2(a). This field sweep is from here on referred to as the negative field sweep. At the reversal field  $H_R$ , the direction of magnetic field sweep is reversed and swept back to  $H_{\text{Sat}}$  following the red solid line while collecting magnetization  $M(H_R, H_Z)$  data. This field sweep is from here on referred to as the positive field sweep. Multiple FORCs are repeated for the desired range of  $H_R$  to compute the FORC distribution  $\rho$  given by the equation  $\rho = -(\partial^2 M / \partial H_R \partial H_Z) / 2$ . Figures 2(b)–2(d) shows the contour plot of  $\rho$  referred to as the FORC diagrams for temperatures of  $19.0^\circ\text{C}$ ,  $23.0^\circ\text{C}$ , and  $26.0^\circ\text{C}$ , respectively [44]. Irreversible transitions are identified from regions of nonzero  $\rho$  on the FORC diagram. Figure 2(b) shows the two main features of magnetic skyrmions that are an upper peak at  $H_R \approx 15$  Oe and a lower trough-peak pair at  $H_R \approx 20$  Oe. By comparing Figs. 2(b)–2(d), these features translated in the negative  $H_Z$  direction with increasing temperature, implying that the single remaining

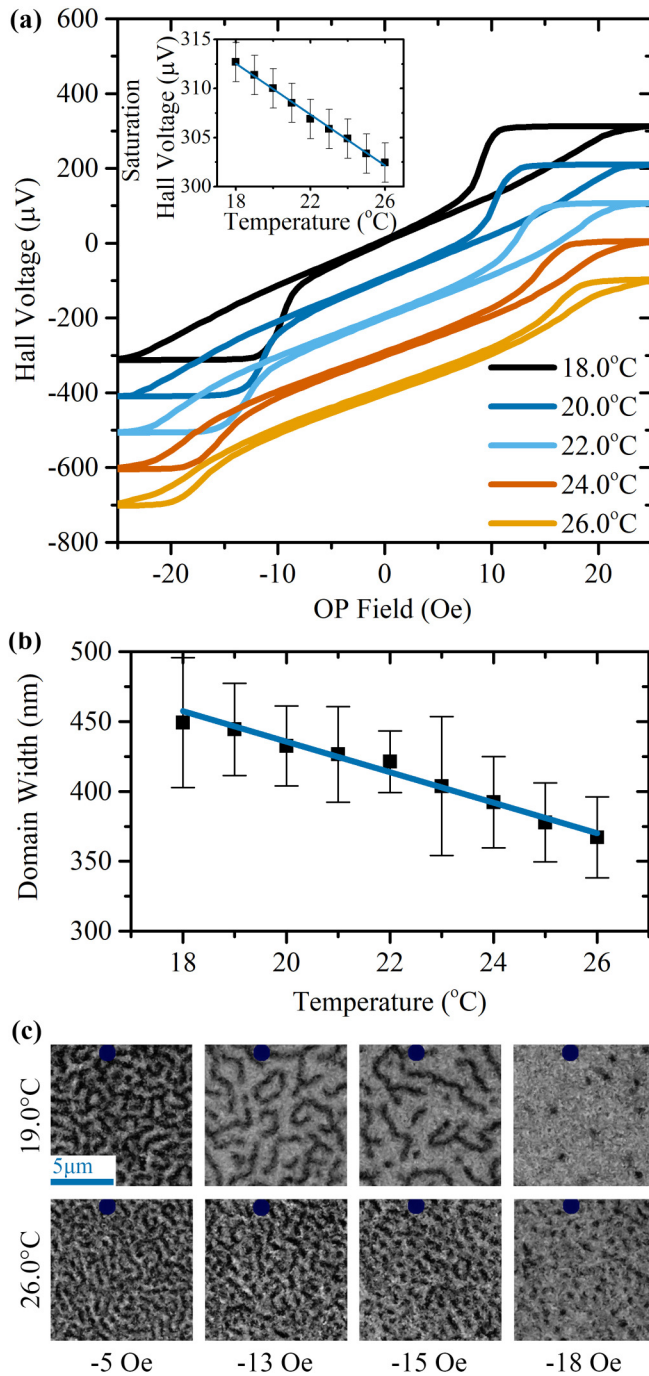


FIG. 1. (a) Out-of-plane magnetic hysteresis. Each curve has an offset of  $-100 \mu\text{V}$  to improve the clarity of the transformation. Inset is the plot of the Hall voltage amplitude at saturation against temperature. (b) Domain width of demagnetized domains. (c) MOKE images after a magnetic field sweep from a negative saturated state to the corresponding positive field at the temperature of  $19.0^{\circ}\text{C}$  and  $26.0^{\circ}\text{C}$ . Dark blue circles obscure defects to avoid misinterpretation as data.

peak at  $26.0^{\circ}\text{C}$  corresponds to the same peak of the trough-peak pair at  $19.0^{\circ}\text{C}$ . The irreversible transition associated with a single peak or trough of  $\rho$  can only be fully described as the combination of two switching events, one associated with each field sweep. The emergence of a peak or trough is

analyzed as a cause-effect relation, where a switching event during the negative field sweep alters the subsequent switching event during the positive field sweep.

### C. Skyrmion transformations at FORC features

Using *in situ* MOKE imaging, the domain transformations are identified along the three key magnetic field sweeps indicated in Figs. 2(b) and 2(d), the negative field sweep represented as a blue dashed line along the diagonal and the two positive field sweeps which intersect the upper peak and the lower trough-peak pair represented as horizontal red dashed lines. To verify that the domain transformation associated with each peak is consistent, MOKE images at  $19.0^{\circ}\text{C}$  for isolated skyrmions and  $26.0^{\circ}\text{C}$  for the skyrmion lattice were captured. Additional supporting MOKE images for  $19.0^{\circ}\text{C}$ ,  $23.0^{\circ}\text{C}$ , and  $26.0^{\circ}\text{C}$  are available in the Supplemental Material [45].

The magnetic domains along the negative field sweep up to the  $H_R$  of the upper peak shown in Fig. 3(c) for  $19.0^{\circ}\text{C}$  and 3(f) for  $26.0^{\circ}\text{C}$ , both show stripe domains fracturing into shorter segments and skyrmions, leaving a mixture of stripe and skyrmions. However, the domains in Fig. 3(c) are far apart with sparse skyrmions, while skyrmion density is significantly larger in Fig. 3(f) and maintains domain-domain separation close to its terminal separation. Terminal separation refers to the minimum stable gap between skyrmions or stripes. This gap is analogous to the domain width approached by the wider domain in a labyrinth with increasing magnetic field in previous works [42,43]. Under a sufficiently large magnetic field, domain-domain separation diverges beyond this terminal width and approaches saturation. At the higher  $H_R$  of the lower peak, Figs. 3(c) and 3(f) both show the process of skyrmion annihilation from a pure skyrmion state. This process is fully consistent between both temperatures, but Fig. 3(f) shows smaller skyrmions and significantly larger skyrmion density.

For the positive field sweep of the upper peak from  $H_R = -16\text{Oe}$  shown in Fig. 3(d) for  $19.0^{\circ}\text{C}$  and  $H_R = -15\text{Oe}$  shown in Fig. 3(g) for  $26.0^{\circ}\text{C}$ , both showed the increase in stripe domains at the expense of skyrmion annihilation as  $H_Z$  is swept past the FORC peak. However, the transformation in Fig. 3(d) involves a significant increase in domains as the stripes propagate to fill the gaps between the domains while the domains in Fig. 3(g) that were initially close to terminal separation showed little change in domain area due to skyrmion-to-stripe transformation. A maximum rate of domain propagation is also associated with the field of  $H_Z = -13\text{Oe}$  where  $\rho$  is maximum at  $19.0^{\circ}\text{C}$ .

For the positive field sweep of the lower peak from  $H_R = -20\text{Oe}$  shown in Fig. 3(e) for  $19.0^{\circ}\text{C}$  and  $H_R = -21\text{Oe}$  shown in Fig. 3(h) for  $26.0^{\circ}\text{C}$ , both transformations began from a pure skyrmions state at their  $H_R$  and subsequently approached the terminal separation as  $H_Z$  was swept across the FORC peak. However, at  $19.0^{\circ}\text{C}$  the skyrmions elongate into stripe domains to fill the sample and approach terminal separation as shown in Fig. 3(e). In this process, the skyrmions were annihilated by transformation into stripes resulting in negligible skyrmion density at the final field. In contrast, skyrmion nucleation occurred to fill the gaps at  $26.0^{\circ}\text{C}$ . For the FORC trough found at  $19.0^{\circ}\text{C}$  with  $H_R = -20\text{Oe}$ , no significant

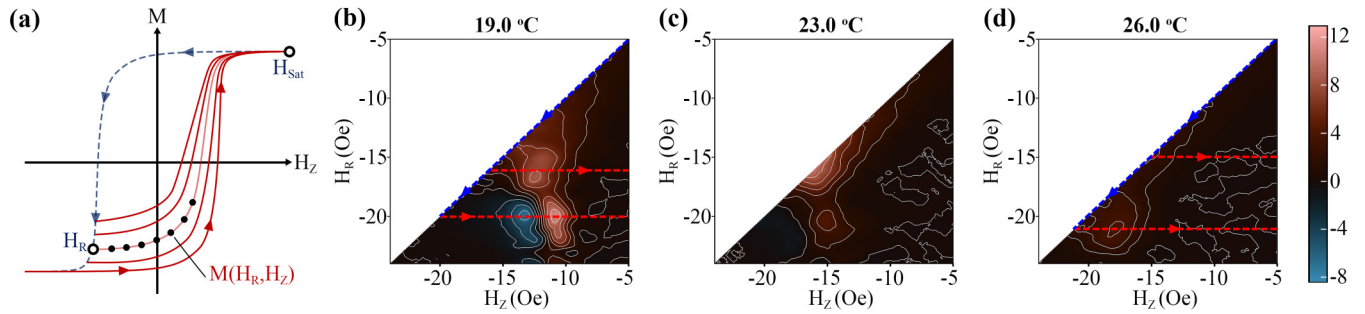


FIG. 2. (a) Schematic for the field sweeps of FORC measurement. (b)–(d) Contour plot of FORC distribution at 19.0 °C, 23.0 °C, and 26.0 °C, respectively. The blue and red dashed lines in (b) and (d) indicate the field sweeps of interest for analysis.

change to the initial pure skyrmions state was observed for  $H_Z < -15$  Oe. As  $H_Z$  was further increased, transformations shown in Fig. 3(e) commenced in tandem with the emergence of the trough.

The plot of FORCs as colored lines based on  $\rho$  in Fig. 3(a) shows that the peaks and trough arise from the convergence and the divergence of the FORCs, respectively. The converging FORCs here correspond to the nucleation of new domains or the propagation of existing domains towards a densely packed state with terminal domain separation as shown in Figs. 3(d), 3(e), and 3(h). The state with terminal separation is identified by the uniformity of the domain-domain separation across the sample that converges to the terminal value. At terminal separation, there are no wide regions in the ferromagnetic state available for expansion, and domains can only further expand by coalescence. The diverging FORCs arise from the process of stripe domain formation and elongation from a limited number of residual skyrmions [46]. The large separation between the residual skyrmions and low skyrmion nucleation rates during the field sweep leads to the amount of stripe domains formed from these residual skyrmions becoming strongly dependent on the number of residual skyrmions at the reversal field  $H_R$ .

Based on the analysis of the domain images,  $H_R$  and  $H_Z$  of the peaks correspond to processes across the whole region of nonzero  $\rho$  associated with the peak rather than domain states at the peak. The upper peak's  $H_R$  corresponds to the fracturing of stripe domains into a mixture of stripes and skyrmions while the upper peak's  $H_Z$  corresponds to the propagation of stripes towards terminal separation. The lower peak's  $H_R$  corresponds to the annihilation of skyrmions from a pure skyrmion state while the lower peak's  $H_Z$  corresponds to the skyrmion nucleation or stripe propagation towards terminal separation. The  $H_Z$  of both peaks represent the transition towards terminal separation, and the domains were observed to reach terminal separation at the edge of the peak where  $\rho$  becomes zero.

While previous works had identified the fracturing and annihilation process during the negative field sweep [35–38,47–49], the lack of analysis of the process associated with the positive field sweep can lead to incomplete descriptions of the peaks. One main contradiction is the process of stripe fracturing into multiple shorter segments or skyrmions that continues to occur even when the upper peak had been almost completely translated off the FORC diagram. From the analysis of the sweeping field, the translation of the upper peak

towards negative  $H_Z$  and its eventual disappearance directly relates to the extent of domain-domain separation divergence from terminal separation, while the process associated with the reversal field continues to occur. The irreversible process of stripe fracturing into skyrmions persisting as seen from their zero-field skyrmion density dependence on  $H_R$  with minimal FORC features highlights the limitation of the FORC technique in quantifying microscopic irreversible domain transformations using the macroscopic measurement of magnetization. However, ironically at the same time demonstrating the high sensitivity of the FORC technique that remains useful even with just a small residual peak.

#### D. Skyrmion phase model

Figure 4 serves as a useful model for the changes in FORC features with respect to magnetic skyrmion phase and stability. With the skyrmion stability parameter  $\kappa$  being strongly dependent on temperature, the horizontal axis in Fig. 4 can be assumed to be analogous with  $\kappa$ .  $H_Z$  of the upper and lower peaks form a pair of linearly decreasing parallel lines, but  $H_Z$  of the upper peak converges to its corresponding  $H_R$  above the temperature of 22.0 °C.  $H_R$  of the lower peak increased and upper peak decreased with temperature, respectively, at a slow rate. The divergence of the upper peak's  $H_R$  and  $H_Z$  at lower temperatures is associated with the isolated skyrmion phase as it represents the existence of a field range where domains remain insensitive to field changes and is far from terminal separation after being fractured into shorter stripe segments or undergone skyrmion annihilation. At high temperatures, the translation of the upper peak towards the negative  $H_Z$  direction and eventually off the FORC diagram represents the decreasing divergence from terminal separation as domain wall energy decreases leading to the domains being stabilized up to larger fields. This model is applicable to the class of magnetic skyrmions stabilized in magnetic multilayers by the combination of interfacial-DMI and dipolar interactions. These magnetic skyrmions exhibit the state transitions between the labyrinth, stripe, skyrmion, and saturated states with a magnetic field and typically have the bow-tie-shaped major hysteresis loop [26,50].

As the upper peak represents the process of skyrmion fracturing and the lower peak being in the pure skyrmion state, a critical field above which stripes are fully annihilated lies between them. The valley which refers to the field of minimum  $\rho$  as projected onto the reversal field showed alignment with

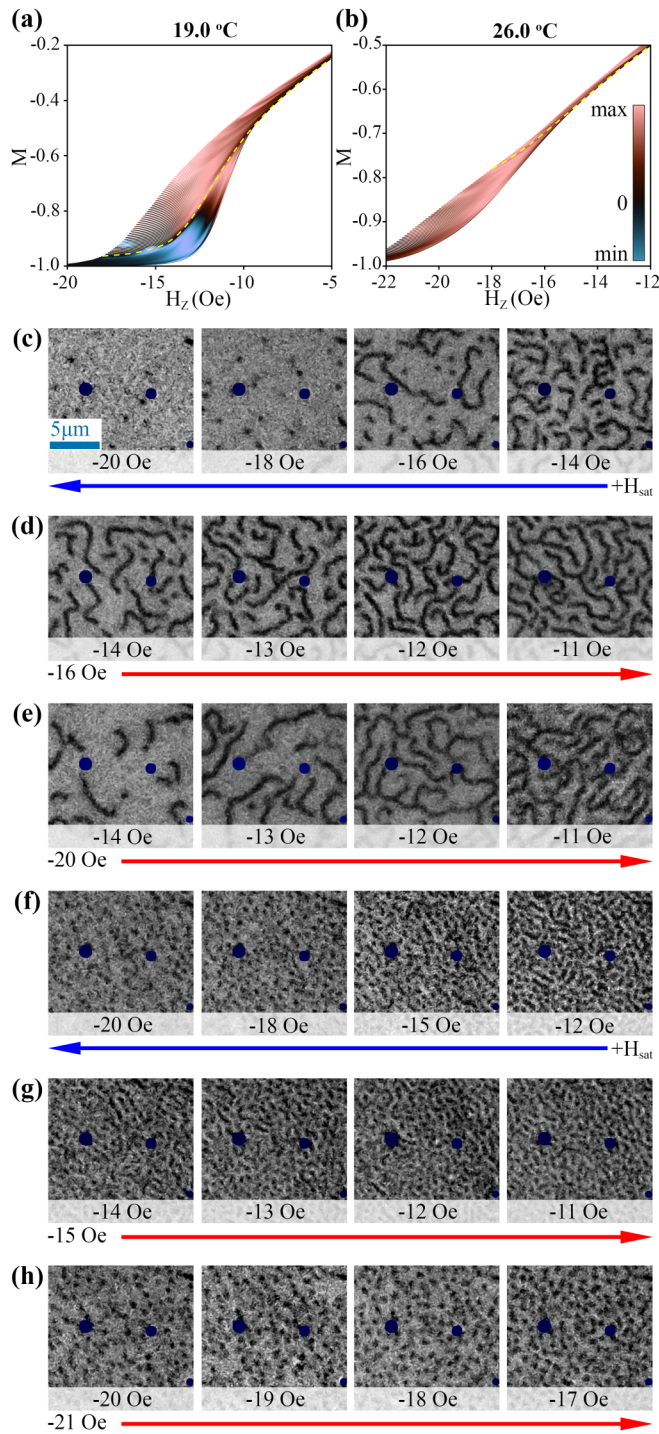


FIG. 3. (a), (b) Plot of colored reversal curves based on the FORC distribution. (c)–(h) MOKE images of the domains during field sweep from the initial or reversal field labeled at the start of the arrows at (c)–(e) 19.0 °C and (f)–(h) 26.0 °C. Blue arrows represent negative field sweeps and red arrows indicate field sweeps. Dark blue circles obscure defects to avoid misinterpretation of data.

the MOKE images for the minimum reversal field for the pure skyrmion state. The lower edge of the bottom peak represents the reversal field for true saturation where all skyrmions are annihilated. The true saturation field is typically larger than that derived from a major hysteresis loop due to the negligible

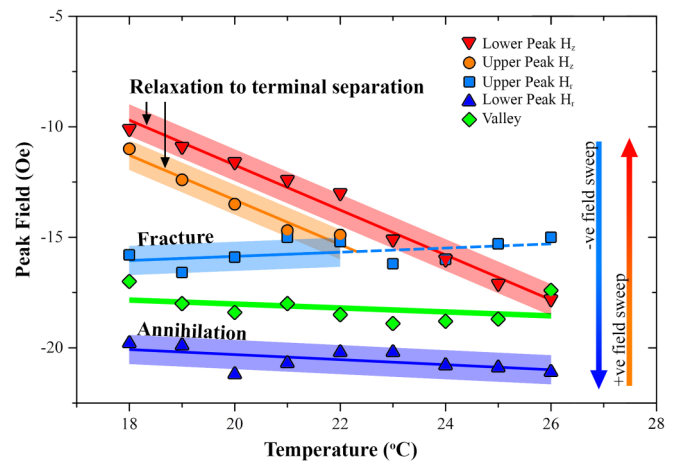


FIG. 4. Plot of the fields of the FORC distribution peaks against temperature. All plots are linearly fitted. The bars signify the processes occur across a range of field. The valley represents the field of minimum FORC distribution between the peaks as projected onto the reversal field. Above 22 °C, the upper peak  $H_z$  converges to its  $H_R$  plotted as the dotted line.

magnetization signal by residual skyrmions close to saturation but these residual skyrmions can induce clear FORC peaks.

Our work provides an intuitive form of analysis for the otherwise abstract FORC distribution and showed its applicability in determining skyrmion phases with the inclusion of the  $H_z$ . In addition to the analysis of magnetic skyrmion phases, FORC identifies the range of fields important for various purposes such as maintaining a pure skyrmion state, the complete annihilation of all domains, and skyrmion-to-stripe transformation which will be key in the development of future skyrmionic devices.

#### IV. CONCLUSION

In conclusion, we report the two peaks in the FORC distribution of a skyrmion sample to correspond to the fracturing of stripe domains and the annihilation of skyrmions for the upper and lower peak, respectively, at the reversal field. Both the peaks correspond to the propagation and/or nucleation of domains to reach terminal domain separation at the sweeping field. Divergence from terminal domain separation is found to be essential for the microscopic domain transformations to develop macroscopic irreversibility detectable *via* the FORC technique. Based on both the reversal field and sweeping field of the FORC distribution peaks, a model was developed to describe FORCs transitioning from isolated skyrmions to the skyrmion lattice phase. Our study clarifies the significance of the FORC features to characterize skyrmion phases and derive useful magnetic field ranges for the desired magnetic state and transformations, which is beneficial to the advancement of research on magnetic skyrmions.

#### ACKNOWLEDGMENTS

This work was supported by the Singapore National Research Foundation, Prime Minister's Office under a Competitive Research Programme (Non-volatile Magnetic Logic

and Memory Integrated Circuit Devices, NRF-CRP9-2011-01), and an Industry-IHL Partnership Program (NRF2015-

IIP001-001). The support from a RIE2020 ASTAR AME IAF-ICP Grant (No. I1801E0030) is also acknowledged.

- [1] A. Fert, V. Cros, and J. Sampaio, *Nat. Nanotech.* **8**, 152 (2013).
- [2] N. Nagaosa and Y. Tokura, *Nat. Nanotech.* **8**, 899 (2013).
- [3] R. Wiesendanger, *Nat. Rev. Mater.* **1**, 16044 (2016).
- [4] A. Fert, N. Reyren, and V. Cros, *Nat. Rev. Mater.* **2**, 17031 (2017).
- [5] X. Zhang, Y. Zhou, K. Mee Song, T.-E. Park, J. Xia, M. Ezawa, X. Liu, W. Zhao, G. Zhao, and S. Woo, *J. Phys. Condens. Matter* **32**, 143001 (2020).
- [6] G. Yu, P. Upadhyaya, Q. Shao, H. Wu, G. Yin, X. Li, C. He, W. Jiang, X. Han, P. K. Amiri *et al.*, *Nano Lett.* **17**, 261 (2017).
- [7] R. Lo Conte, A. K. Nandy, G. Chen, A. L. Fernandes Cauduro, A. Maity, C. Ophus, Z. Chen, A. T. N'Diaye, K. Liu, A. K. Schmid *et al.*, *Nano Lett.* **20**, 4739 (2020).
- [8] C. C. I. Ang, W. Gan, and W. S. Lew, *New J. Phys.* **21**, 043006 (2019).
- [9] S. Luo, M. Song, X. Li, Y. Zhang, J. Hong, X. Yang, X. Zou, N. Xu, and L. You, *Nano Lett.* **18**, 1180 (2018).
- [10] M. Chauwin, X. Hu, F. Garcia-Sanchez, N. Betrabet, A. Paler, C. Moutafis, and J. S. Friedman, *Phys. Rev. Appl.* **12**, 064053 (2019).
- [11] M. G. Mankalale, Z. Zhao, J. Wang, and S. S. Sapatnekar, *IEEE Trans. Electron Devices* **66**, 1990 (2019).
- [12] S. Luo, M. Song, M. Shen, Y. Zhang, J. Hong, and L. You, *J. Magn. Magn. Mater.* **494**, 165739 (2020).
- [13] F. Garcia-Sanchez, J. Sampaio, N. Reyren, V. Cros, and J. V. Kim, *New J. Phys.* **18**, 075011 (2016).
- [14] D. Fan, Z. He, and S. Angizi, in *2017 IEEE 60th International Midwest Symposium on Circuits and Systems* (Medford, MA, United States, 2017), p. 1109.
- [15] Z. He and D. Fan, in *Design, Automation & Test in Europe Conference & Exhibition (DATE)* (Lausanne, Switzerland, 2017), p. 350.
- [16] M. A. Azam, D. Bhattacharya, D. Querlioz, and J. Atulasimha, *J. Appl. Phys.* **124**, 152122 (2018).
- [17] X. Chen, W. Kang, D. Zhu, X. Zhang, N. Lei, Y. Zhang, Y. Zhou, and W. Zhao, *Nanoscale* **10**, 6139 (2018).
- [18] D. Pinna, F. Abreu Araujo, J. V. Kim, V. Cros, D. Querlioz, P. Bessiere, J. Droulez, and J. Grollier, *Phys. Rev. Appl.* **9**, 064018 (2018).
- [19] J. Zázvorka, F. Jakobs, D. Heinze, N. Keil, S. Kromin, S. Jaiswal, K. Litzius, G. Jakob, P. Virnau, D. Pinna *et al.*, *Nat. Nanotech.* **14**, 658 (2019).
- [20] I. Dzyaloshinsky, *J. Phys. Chem. Solids* **4**, 241 (1958).
- [21] P. W. Anderson, *Phys. Rev.* **115**, 2 (1959).
- [22] T. Moriya, *Phys. Rev.* **120**, 91 (1960).
- [23] M. Ezawa, *Phys. Rev. Lett.* **105**, 197202 (2010).
- [24] Y. Tokura and N. Kanazawa, *Chem. Rev.* **121**, 2857 (2020).
- [25] A. Bernand-Mantel, C. B. Muratov, and T. M. Simon, *Phys. Rev. B* **101**, 045416 (2020).
- [26] A. Soumyanarayanan, M. Raju, A. L. Gonzalez Oyarce, A. K. C. Tan, M.-Y. Im, A. P. Petrović, P. Ho, K. H. Khoo, M. Tran, C. K. Gan *et al.*, *Nat. Mater.* **16**, 898 (2017).
- [27] C. Moreau-Luchaire, C. Moutafis, N. Reyren, J. Sampaio, C. A. F. Vaz, N. Van Horne, K. Bouzehouane, K. Garcia, C. Deranlot, P. Warnicke *et al.*, *Nat. Nanotech.* **11**, 444 (2016).
- [28] I. Lemesh and G. S. D. Beach, *Phys. Rev. B* **98**, 104402 (2018).
- [29] A. Bogdanov and A. Hubert, *J. Magn. Magn. Mater.* **138**, 255 (1994).
- [30] S. Rohart and A. Thiaville, *Phys. Rev. B* **88**, 184422 (2013).
- [31] A. Siemens, Y. Zhang, J. Hagemeister, E. Y. Vedmedenko, and R. Wiesendanger, *New J. Phys.* **18**, 045021 (2016).
- [32] T. Srivastava, W. Lim, I. Joumard, S. Auffret, C. Baraduc, and H. Béa, *Phys. Rev. B* **100**, 220401(R) (2019).
- [33] S. Zhang, J. Zhang, Y. Wen, E. M. Chudnovsky, and X. Zhang, *Appl. Phys. Lett.* **113**, 192403 (2018).
- [34] D. A. Garanin, E. M. Chudnovsky, S. Zhang, and X. Zhang, *J. Magn. Magn. Mater.* **493**, 165724 (2020).
- [35] A. S. Westover, K. Chesnel, K. Hatch, P. Salter, and O. Hellwig, *J. Magn. Magn. Mater.* **399**, 164 (2016).
- [36] N. K. Duong, M. Raju, A. P. Petrović, R. Tomasello, G. Finocchio, and C. Panagopoulos, *Appl. Phys. Lett.* **114**, 072401 (2019).
- [37] M. Ma, C. C. I. Ang, Y. Li, Z. Pan, W. Gan, W. S. Lew, and F. Ma, *J. Appl. Phys.* **127**, 223901 (2020).
- [38] N. K. Duong, R. Tomasello, M. Raju, A. P. Petrović, S. Chiappini, G. Finocchio, and C. Panagopoulos, *APL Mater.* **8**, 111112 (2020).
- [39] B. J. Kirby, J. E. Davies, K. Liu, S. M. Watson, G. T. Zimanyi, R. D. Shull, P. A. Kienzle, and J. A. Borchers, *Phys. Rev. B* **81**, 100405 (2010).
- [40] J. E. Davies, O. Hellwig, E. E. Fullerton, G. Denbeaux, J. B. Kortright, and K. Liu, *Phys. Rev. B* **70**, 224434 (2004).
- [41] B. Buford, P. Dhagat, and A. Jander, *IEEE Magn. Lett.* **7**, 6507305 (2016).
- [42] I. Lemesh, F. Büttner, and G. S. D. Beach, *Phys. Rev. B* **95**, 174423 (2017).
- [43] S. Jaiswal, K. Litzius, I. Lemesh, F. Büttner, S. Finizio, J. Raabe, M. Weigand, K. Lee, J. Langer, B. Ocker *et al.*, *Appl. Phys. Lett.* **111**, 022409 (2017).
- [44] F. Cramer, *Geosci. Model Dev.* **11**, 2541 (2018).
- [45] See Supplemental Material at <http://link.aps.org/supplemental/10.1103/PhysRevB.103.144409> for additional data on temperature dependence of FORC distribution and supporting MOKE images for skyrmion transformations at each FORC peak.
- [46] J. E. Davies, O. Hellwig, E. E. Fullerton, M. Winklhofer, R. D. Shull, and K. Liu, *Appl. Phys. Lett.* **95**, 022505 (2009).
- [47] A. K. C. Tan, J. Lourembam, X. Chen, P. Ho, H. K. Tan, and A. Soumyanarayanan, *Phys. Rev. Mater.* **4**, 114419 (2020).
- [48] X. Wang, Y. Wei, K. He, Y. Liu, Y. Huang, Q. Liu, J. Wang, and G. Han, *J. Phys. D* **53**, 215001 (2020).
- [49] D. Toneto, R. B. da Silva, L. S. Dorneles, F. Béron, S. Oyarzún, and J. C. Denardin, *J. Phys. D* **53**, 395001 (2020).
- [50] S. D. Pollard, J. A. Garlow, J. Yu, Z. Wang, Y. Zhu, and H. Yang, *Nat. Commun.* **8**, 14761 (2017).